Journal of Crystal Growth 311 (2009) 1791–1794

Contents lists available at ScienceDirect

Journal of Crystal Growth

journal homepage: www.elsevier.com/locate/jcrysgro

The effects of rapid thermal annealing on doubled quantum dots grown by molecular beam epitaxy

S. Suraprapapich [a,b,c,*], Y.M. Shen [a], Y. Fainman [a], Y. Horikoshi [c], S. Panyakeow [b], C.W. Tu [a]

[a] Department of Electrical and Computer Engineering, University of California San Diego, La Jolla, CA 92093-0407, USA
[b] Department of Electrical Engineering, Chulalongkorn University, Phayathai Road, Patumwan, Bangkok 10330, Thailand
[c] Kagami Memorial Laboratory for Material Science and Technology, Waseda University, Tokyo 169-0051, Japan

ARTICLE INFO

Available online 24 December 2008

Keywords:
A1. Double quantum dot
A1. Rapid thermal annealing
A3. Molecular beam epitaxy

PACS:
00

ABSTRACT

The effects of different rapid thermal annealing temperatures on the optical properties of InAs double quantum dots (DQDs) grown by molecular beam epitaxy using a partial-capping-and-regrowth process have been investigated. Improvement of the material quality is indicated by enhanced photoluminescence (PL) intensity and narrower PL linewidth. The blueshift of the PL emission peak with increasing annealing temperature is due to the interdiffusion of group III atoms during the annealing process, which is confirmed by the temperature dependence of the PL peak position. Thermal quenching of the PL intensity is observed at temperature over 110 K, and the main activation energy decreases with annealing temperature, consistent with a reduced confining potential from the interdiffusion of group III atoms. All of these results are similar to those of single quantum dots reported in the literature.

1. Introduction

Self-assembled quantum dots (SA-QDs) by the Stranski–Krastanow (S–K) growth mode have attracted much attention due to their interest in both unique atomic-like properties and potential device applications [1–5]. In quantum information processing, a key building block of a quantum processor is a quantum gate, which is used to entangle the states of two quantum bits (qubits) [6–7]. Recently, a pair of aligned semiconductor QDs has been used as an optically driven quantum gate [8]. To date, vertically aligned double QDs (DQDs) have been fabricated by cleaved-edge overgrowth or the growth of upper SA-QDs on top of lower SA-QDs due to the strain field around the lower QDs [9–11]. In principle, lateral DQDs are preferred as they allow a large number of quantum gates realized in a two-dimensional array. Lateral DQDs have been successfully fabricated by several growth methods such as droplet epitaxy or a combination of self-assembly with in situ etching [12,13]. Recently, we have produced SA InAs DQDs on a GaAs (0 0 1) substrate under As_2 overpressure using a partial-capping-and-regrowth technique by molecular beam epitaxy (MBE) [14,15].

There are many applications requiring controlled emission peaks and narrow emission linewidth; for example, DQDs could be used in quantum computing by putting them into a cavity structure. Because it is difficult to tune the resonance energy of the cavity after fabrication, rapid thermal annealing (RTA) may become a promising way to tune the emission energy of the DQDs to match the resonance of the cavity [16]. Moreover, RTA has also been used to reduce the number of point defects.

In this article, we investigate the effect of the RTA process on the photoluminescence (PL) spectra of DQDs with various annealing temperatures. Furthermore, thermal activation of localized excitons is studied using temperature-dependent PL spectroscopy for as-grown DQDs and their behavior upon post-growth rapid thermal treatment.

2. Experimental procedure

All samples are grown on (0 0 1) semi-insulating GaAs substrates under As_2 overpressure by MBE. The growth rates of GaAs and InAs are 0.6 and 0.01 monolayer (ML) per second, respectively. After oxide desorption, a 300-nm-thick GaAs buffer layer is grown at a temperature of 580 °C. Next, with deposition of 1.8 ML amount of InAs, QDs are formed randomly on the surface at a temperature of 500 °C. Then, the substrate temperature is ramped down to 470 °C and the InAs QDs are capped partially with a 6-ML-thick GaAs layer. Then, additional 0.6-ML-thick InAs is deposited, and DQDs are formed. After that, a 150-nm-thick GaAs buffer layer is grown. These embedded DQDs are for PL measurements. The partial-capping-and-regrowth process is repeated once more on top of the structure for AFM measurements. The dot formation is monitored *in situ* by

*Corresponding author at: Department of Electrical Engineering, Chulalongkorn University, Phayathai Road, Patumwan, Bangkok10330, Thailand.
E-mail address: suwaree2001@yahoo.com (S. Suraprapapich).

0022-0248/$ - see front matter © 2008 Elsevier B.V. All rights reserved.
doi:10.1016/j.jcrysgro.2008.12.037

reflection high-energy-electron diffraction (RHEED). After growth the sample is ramped down immediately to room temperature.

The effect of postgrowth RTA, in nitrogen ambient at temperature of 650, 700, 750, 800 and 850 °C, on the optical properties of DQDs is investigated. The annealing time is 30 s for each. Unannealed DQD samples are designated as "as-grown DQDs".

The surface morphology is imaged by tapping-mode AFM with a sharpened SiN tip on uncapped samples. Photoluminescence spectra are measured in a close-cycle He cryostat at various temperatures from 9 K to room temperature. A diode-pumped solid-state laser at 532 nm emission wavelength is used for excitation, and the collected PL is dispersed by a 0.5 m monochromator and detected by a thermoelectrically cooled InGaAs photodiode using a standard lock-in detection technique.

The structural property of as-grown DQDs sample is analyzed by cross-section transmission electron microscopy (TEM). The TEM measurement is carried out with a 200 kV electron beam on the sample, which is milled by focused ion beam (FIB) for electron transparency.

3. Results and discussion

Fig. 1 shows an AFM image of as-grown DQDs fabricated by MBE under As_2 overpressure. Each as-grown QD in the first SA-QD layer is transformed into a quantum ring after partial-capping with 6 ML of GaAs. When additional 0.6 ML of InAs is deposited, DQDs are formed, with the two QDs oriented along the $[1\bar{1}0]$ crystallographic direction [14]. The total QD density is $1.1 \times 10^{10}\,cm^{-2}$, consisting of 80% DQDs and 20% single dots. The average dot height is ~4 nm and center-to-center spacing is ~22 nm [14].

In order to understand the DQD structure, cross-sectional TEM is performed, as shown in Fig. 2. We can see the two wetting layers and profiles of DQDs. It is interesting to note that the lower quantum rings seem to have transformed into DQDs as well. The structure of the lower DQDs needs further high-resolution TEM investigations.

Fig. 3 shows low-temperature PL spectra of as-grown and annealed DQDs (at 650, 750 and 850 °C). The increase in the PL emission intensity up to 750 °C is most likely a result of curing of point defects formed from low-temperature growth. For the as-grown DQD sample, the emission peak is 1.198 eV with a full-width at half-maximum (FWHM) of 61 meV. The peak position of annealed DQDs at 650, 750 and 850 °C are blueshifted from the as-grown DQDs by 13, 47 and 102 meV, respectively, and the FWHM decreases to 59, 42 and 33 meV, respectively. Both the blueshift and narrowing of FWHM can be explained by the interdiffusion of In and Ga atoms at the interface between the InAs QD and the GaAs barrier. Mixing Ga into InAs increases the energy bandgap inside the individual QDs, while diffusion of In into the GaAs barrier smoothes the confining potential for charge carriers. Both of these effects result in the observed blue shift. The line width of the PL peak is due to inhomogeneous broadening from QD size distribution. For a given annealing temperature and the resultant diffusion length, intermixing will have a stronger effect on the smaller QDs. As the annealing temperature is increased, the confining potential becomes shallower, resulting in a narrowing of the inhomogeneous broadening [16].

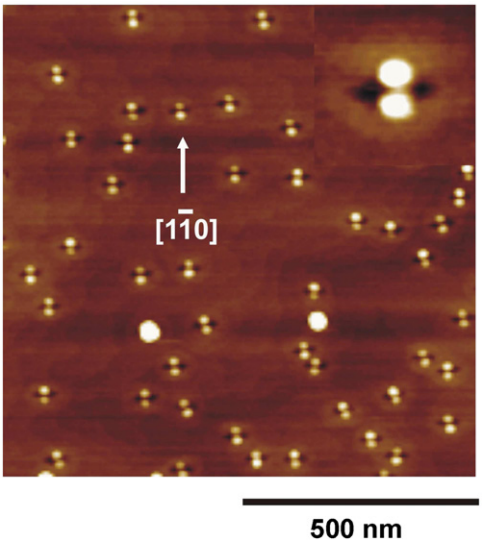

Fig. 1. AFM image of as-grown DQDs. The inset is high-contrast image.

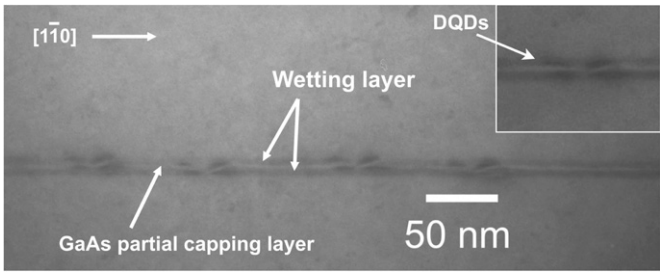

Fig. 2. Cross-sectional TEM image of DQDs using partial-capping-and-regrowth process.

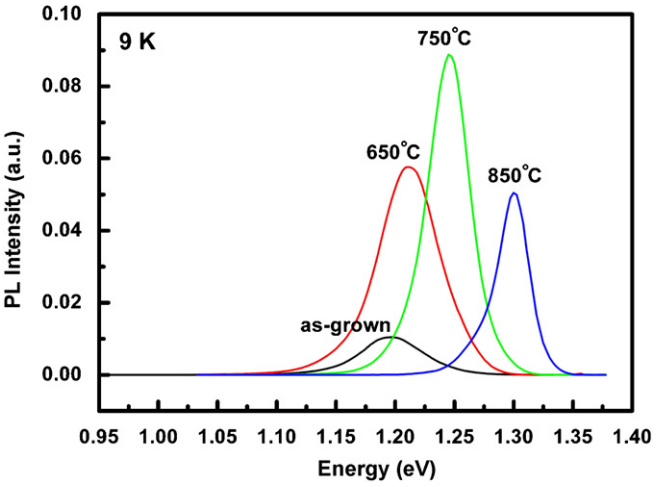

Fig. 3. PL spectra at 9 K of as-grown DQDs and samples annealed at different temperatures of 650, 750 and 850 °C for 30 s.

Temperature-dependent PL data are measured from 9 to 290 K with 50 mW incident excitation power from a diode-pumped solid-state laser at 532 nm. The PL peak energy as a function of sample temperature is shown in Fig. 4, and fitting curves are plotted (solid lines) using the Varshni equation [17]

$$E(T) = E_0 - \frac{\alpha T^2}{T + \beta} \quad (1)$$

where $E(T)$ and E_0 are the peak energies at T and 0 K, respectively, and α and β are constants. In the case of the annealed sample at 650 °C, the PL data can be fitted well by Eq. (1) with α=3.6 × 10^{-4} eV/K and β=150 K. These values lie between those of bulk InAs and GaAs. This further confirms the existence of

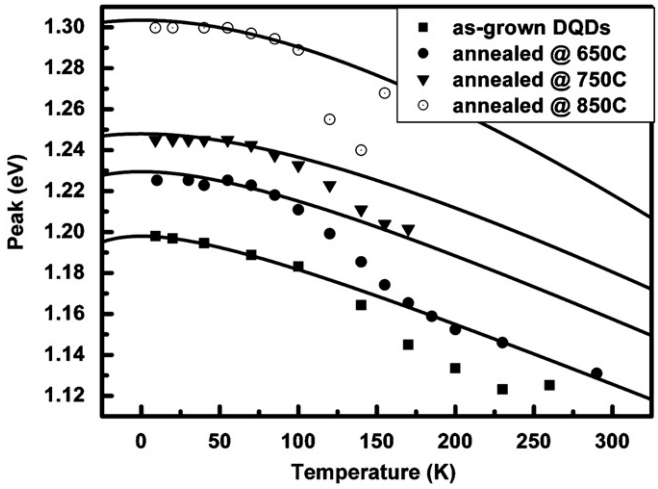

Fig. 4. The temperature-dependence curves of the PL peak energies of as-grown DQDs and samples at different annealing temperatures. The solid lines are fitted by the Varshni equation.

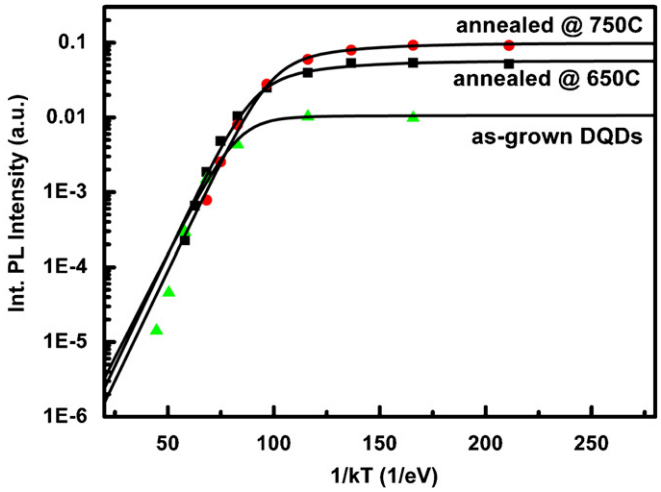

Fig. 5. Integrated PL intensities of as-grown DQDs and thermally annealed DQDs at 650 and 750 °C as a function of inverse temperature.

interdiffusion between Ga and In during the annealing process. This is because even though the bandgap of QDs is dominated by strain and quantum confinement, the confined energy levels of the QD follow the conduction and valence band edge of the constituent material. However, the emission peak energy vs. temperature data generally follow the Varshni equation only below 100 K. Above 100 K, the emission peak energy is lower. This can be explained as follows. The Varshni equation describes the bandgap change in a single dot. When the temperature increases, the electrons can diffuse more easily to larger-size, lower-energy QDs, resulting in dominant PL from the larger QDs.

Fig. 5 shows the PL intensity of as-grown and annealed DQDs as a function of inverse temperature. At lower temperatures up to 100 K for as-grown DQDs and up to 85 K for annealed samples, the PL intensity is almost unchanged under a constant flux of electron–hole pairs generated in the samples and it monotonically decreases at high temperatures. It is interesting to note that the quenching temperature in annealed samples occur earlier compared with as-grown DQDs due to the smaller confinement potential barrier. At low temperature, the PL intensity remains almost constant with temperature, which indicates that the barriers are relatively high compared to the value corresponding to the measurement temperature. However, at the high temperature range, the carriers have high enough energy to overcome the barrier leading to the quenching of the luminescence. These curves are fitted by [18–19]

$$I(T) = \frac{I(0)}{1 + Ae^{-E_a/kT} + Be^{-E_b/kT}} \quad (2)$$

where $I(T)$ and $I(0)$ are the PL intensity at T and 0 K, respectively; A and B are constants; E_a and E_b are thermal activation energies. For proper fitting, we need to assume two thermally activated processes characterized by E_a and E_b. Activation energy E_a, derived from the slopes of the straight-line portion (150–300 K) of the curves, is 130 meV for as-grown DQDs and 75 meV for the sample annealed at 650 °C. Activation energy E_b of all samples, determined by curve fitting, is in the range 25–30 meV, independent of annealing temperature. The smaller activation energy of E_b is attributed to trapped excitons or carriers thermalizing from localized regions resulting from potential fluctuation in the QDs. The larger activation energy of E_a of 130 meV for as-grown DQDs is comparable to the difference in energy (~110 meV) between the ground state and the wetting-layer state [20]. The decrease of E_a with increasing annealing temperature can be interpreted as mostly from a reduction in the depth of the confining potential caused by interdiffusion of In and Ga atoms during annealing.

It is noted that the material quality of DQDs is highly improved after annealing in terms of the reduction of nonradiative recombination centers leading to enhanced PL intensity.

4. Conclusion

The effects of thermal annealing on the optical properties of lateral DQDs have been investigated. We observe a stronger PL intensity and narrower linewidth with increasing annealing temperature up to 750 °C, indicating improvement of the material quality. We also observe a blueshift of the PL emission peak with increasing annealing temperature, which is due to the interdiffusion of group III atoms during the annealing process. The temperature dependence of the PL peak position of annealed DQDs, which is fitted with Varshni equation, confirms the group III interdiffusion. Thermal quenching of the PL intensity is observed at temperature over 110 K. The activation energy is observed to decrease with annealing temperature, consistent with a reduced confining potential from the interdiffusion of group III atoms. Because planar samples are investigated, PL probes actually an ensemble of nanostructures, consisting of top DQDs and bottom DQDs (or truncated quantum rings), which are in contact with the two wetting layers in the GaAs matrix. Thus, all of the results obtained are similar to those for single QDs reported in the literature.

Acknowledgments

This work is partially supported by the Quantum Information Science and Technology (QuIST) program of the US Air Force Office of Scientific Research (AFOSR) and the Thailand Research Fund (TRF) Senior Researcher Scholar, Marubun Research Promotion Foundation, Asian Office of Aerospace Research and Development (AOARD) of the US Air Force, Chulalongkorn University and National Nanotechnology Center of Thailand.

References

[1] M. Sugawara, Self-Assembled InGaAs/GaAs Quantum Dots: Semiconductors and Semimetals, vol. 60, Academic Press, New York, 1999.
[2] W. Seifert, N. Carlsson, M. Miller, M.-E. Pistol, L. Samuelson, L.R. Wallenberg, Prog. Cryst and. Growth Charact. 33 (1996) 423.
[3] Y. Arakawa, H. Sakaki, Appl. Phys. Lett. 40 (1982) 939.
[4] M. Asada, Y. Miyamoto, Y. Suematsu, IEEE J. Quantum Electron. QE-22 (1986) 1915.
[5] Y. Wang, S.Y. Chou, Appl. Phys. Lett. 63 (1993) 2257.
[6] S.S. Li, J.B. Xia, J.L. Liu, F.H. Yang, Z.C. Niu, S.L. Feng, H.Z. Zheng, J. Appl. Phys. 90 (2001) 6151.
[7] D.P. Divincenzo, Science 309 (2005) 2173.
[8] L. Robledo, J. Elzerman, G. Jundt, M. Atature, A. Hogele, S. Falt, A. Imamoglu, Science 309 (2005) 2173.
[9] Q. Xie, P. Chen, A. Madhukar, Appl. Phys. Lett. 65 (1994) 2051.
[10] G. Schedelbeck, W. Wesgscheider, M. Bischler, G. Abstreiter, Science 278 (1997) 1792.
[11] S. Yamauchi, K. Komori, T. Sugaya, K. Goshima, Jpn. J. Appl. Phys. 43 (2004) 2083.
[12] R. Songmuang, S. Kiravittaya, O.G. Schmidt, Appl. Phys. Lett. (2003) 2892.
[13] J.H. Lee, Zh.M. Wang, N.W. Strom, Y.I. Mazur, G.J. Salamo, Appl. Phys. Lett. 89 (2006) 202101.
[14] S. Suraprapapich, Y.M. Shen, V.A. Odnoblyudov, Y. Fainman, S. Panyakeow, C.W. Tu, J. Crystal Growth 301 (2007) 735.
[15] S. Suraprapapich, S. Panyakeow, C.W. Tu, Appl. Phys. Lett. 90 (2007) 183112.
[16] A. Rastelli, S.M. Ulrich, E.-M. Pavelescu, T. Leinonen, M. Pessa, P. Michler O.G. Schmidt, Superlattices and Microstructures 36 (2004) 181.
[17] Y.P. Varshni, Physica 34 (1967) 149.
[18] A. Nishikawa, Y.G. Hong, C.W. Tu, J. Vac. Sci. Technol. B 22 (2004) 1515.
[19] D.P. Popescu, P.G. Eliseev, A. Stintz, K.J. Malloy, Semicond. Sci. Technol. 19 (2004) 33.
[20] Z.Y. Xu, Z.D. Lu, X.P. Yang, Z.L. Yuan, B.Z. Zheng, J.Z. Xu, Phys. Rev. B 54 (1996) 11528.